



Cite this: *Energy Environ. Sci.*, 2018, **11**, 417

The role of fullerenes in the environmental stability of polymer:fullerene solar cells†

Harrison Ka Hin Lee,^a Andrew M. Telford,^b Jason A. Röhr,^b Mark F. Wyatt,^{id c} Beth Rice,^b Jiaying Wu,^d Alexandre de Castro Maciel,^{be} Sachetan M. Tuladhar,^b Emily Speller,^a James McGettrick,^a Justin R. Searle,^a Sebastian Pont,^{id d} Trystan Watson,^{id a} Thomas Kirchartz,^{id fg} James R. Durrant,^{id ad} Wing C. Tsoi,^{id a} Jenny Nelson^{id *ab} and Zhe Li^{id *a}

Environmental stability is a common challenge for the commercialisation of low cost, encapsulation-free organic opto-electronic devices. Understanding the role of materials degradation is the key to address this challenge, but most such studies have been limited to conjugated polymers. Here we quantitatively study the role of the common fullerene derivative PCBM in limiting the stability of benchmark organic solar cells, showing that a minor fraction (<1%) of photo-oxidised PCBM, induced by short exposure to either solar or ambient laboratory lighting conditions in air, consistent with typical processing and operating conditions, is sufficient to compromise device performance severely. We identify the effects of photo-oxidation of PCBM on its chemical structure, and connect this to specific changes in its electronic structure, which significantly alter the electron transport and recombination kinetics. The effect of photo-oxidation on device current–voltage characteristics, electron mobility and density of states could all be explained with the same model of photoinduced defects acting as trap states. Our results demonstrate that the photochemical instability of PCBM and chemically similar fullerenes remains a barrier for the commercialisation of organic opto-electronic devices.

Received 17th October 2017,
Accepted 10th January 2018

DOI: 10.1039/c7ee02983g

rsc.li/ees

Broader context

Abundant, low-cost and easily processed materials are urgently needed for applications in energy conversion and storage. In this context, solution processable organic and lead-halide perovskite semiconductors have attracted intense interest for use in solar cells. However, environmental stability of these and other low cost, solution processed electronic devices remains the major challenge for commercialisation. Solving the device stability issue requires methods to identify the causes of degradation (for example, semiconductor or electrode failure, chemical or electrochemical processes) and to relate changes in electrical performance to specific degradation mechanisms. Here, we identify a degradation pathway that is relevant to many designs of organic and perovskite solar cells, namely, the photochemical oxidation of fullerenes under exposure to ambient light, and show that the effects on charge transport, device photovoltage, and current–voltage characteristic can be related quantitatively to the nature and energy of specific oxidised defects introduced by light. These findings challenge the widely held assumption that the photo-degradation of donor polymers is the primary weakness of organic solar cells and show that exposure to ambient laboratory or factory lighting in air may be sufficient to compromise device performance. The work provides a target and a methodology in the pursuit of superior materials for solar cells, namely, that more robust electron transport materials are needed, and that the viability of candidates can be assessed from knowledge of their oxidation products and the predicted effect on device response. The work thus provides a predictive step in the design of environmentally stable devices.

^a SPECIFIC IKC, College of Engineering, Bay campus, Swansea University, Wales, SA1 8EN, UK. E-mail: z.li@swansea.ac.uk

^b Department of Physics, Imperial College London, London, SW7 2AZ, UK. E-mail: jenny.nelson@imperial.ac.uk

^c EPSRC UK National Mass Spectrometry Facility (NMSF), Swansea University Medical School, Wales, SA2 8PP, UK

^d Department of Chemistry, Imperial College London, London, SW7 2A, UK

^e Department of Physics, CCN, Federal University of Piauí, Teresina, 64049-550, Brazil

^f IEK5-Photovoltaics, Forschungszentrum Jülich, 52425 Jülich, Germany

^g Faculty of Engineering and CENIDE, University of Duisburg-Essen, Carl-Benz-Str. 199, 47057 Duisburg, Germany

† Electronic supplementary information (ESI) available. See DOI: 10.1039/c7ee02983g

Introduction

A common challenge for the commercialisation of organic opto-electronic devices such as solar cells is their typically limited environmental stability. Organic solar cells have undergone significant improvements in performance with their efficiencies increasing from 3% to over 13% in the last decade,¹ primarily due to the recent development of a range of high performance donor polymers and non-fullerene acceptors.^{2–4} However, their limited environmental stability and short lifetimes have become a major hurdle for commercialisation.^{5–7} Numerous reports have shown that

exposure to air typically results in rapid deterioration of device performance, especially when combined with exposure to light.^{8,9} A general strategy to address this challenge is using device encapsulation, thereby creating a physical barrier for the diffusion of molecular oxygen into the device and hindering the reaction route of oxygen induced degradation.⁵ However, encapsulation significantly increases the fabrication cost, and despite substantial research efforts,^{10–13} little success has been demonstrated to date in extending the lifetimes of un-encapsulated devices under exposure to light and oxygen. Understanding the degradation mechanisms and enhancing the intrinsic stability of organic opto-electronic devices is therefore of paramount importance for their commercialisation.

The majority of studies of photoactive material stability have addressed the stability of the donor (polymer) component.^{5,6,14,15} Despite their common use in solution-processed optoelectronic devices, fullerenes have been known to be sensitive to photo-induced reactions since the early 1990s.^{16,17} For example, under UV or visible illumination in inert atmosphere, fullerenes such as phenyl-C₆₁-butyric acid methyl ester (PCBM) can form covalent intermolecular C–C bonds to form dimers or higher oligomers. Such photo-oligomerisation has been correlated with a loss of organic photovoltaic (OPV) device efficiency under irradiation (the “burn-in” effect),^{10,18} although modest PCBM photo-oligomerisation can also be beneficial, improving the morphological stability of OPV devices under thermal stress.^{12,19} In the presence of oxygen, PCBM and other fullerene derivatives have been shown to undergo photo-oxidation,²⁰ with two most commonly observed products of photo-oxidation, epoxide and carbonyl, on the fullerene cage.²¹ While the photo-oxidation of fullerenes has been investigated in detail by Moons and co-workers,^{22,23} little has been reported on its effect on the performance of organic opto-electronic devices, and especially on the exact mechanism of performance loss. A small number of studies have shown that organic solar cells containing deliberately photo-oxidised fullerene derivatives exhibit dramatic losses in their performance,^{24,25} but provided no mechanistic explanation, nor proof of relevance to OPV stability. A few groups have suggested the formation of trap states upon fullerene photo-oxidation based on quantum chemical simulations, with limited direct evidence of the relationship of defects to electronic properties.^{26,27}

In this paper, we evaluate the impact of PCBM photo-oxidation on the performance and stability of polymer:fullerene bulk heterojunction devices. We found that a minor fraction of photo-oxidised PCBM in blends films with the benchmark polymer poly[N-9'-heptadecan-2,7-carbazole-*alt*-5,5-(4',7'-di-2-thienyl-2',1',3'-benzothiadiazole)] (PCDTBT), which is the most stable OPV polymer demonstrated so far,²⁸ induced by exposure to only a few minutes of illumination in air, can result in severe degradation of device performance. We systematically investigated the effect of introducing minor fractions (0.2 to 3.6%) of deliberately photo-oxidised PCBM on the transport and recombination mechanisms in OPV devices, to explain the losses in power conversion efficiency (PCE). We extend our conclusions to OPV devices based on other benchmark polymers, namely

P3HT, PTB7, and PTB7-Th. We show that fullerene photo-oxidation can be a primary mechanism dominating the degradation of fullerene-based opto-electronic devices. The highly photoactive nature of fullerenes and strong correlation to device performance suggest that fullerene photo-oxidation must be taken into account in the choice of processing route for fullerene-based electronic devices. The methodology presented here could readily be applied to probe specific degradation pathways in other OPV systems, such as those containing alternative acceptors.

Results

Impact of fullerene photo-oxidation on OPV devices behaviour

We investigated the decrease in performance due to degradation of bulk-heterojunction OPV devices upon exposure to light and oxygen. Previous studies concluded that light and/or oxygen exposure of un-encapsulated devices resulted in rapid device degradation due to diffusion and subsequent reaction of molecular oxygen with the polymer component of the active layer materials.⁵ Fig. 1(a) shows the evolution of current density–voltage (*J*–*V*) characteristics of typical PCDTBT:PCBM devices having undergone different exposure durations to AM 1.5G conditions in air (see also Table S1, ESI†). Exposure prior to electrode deposition allowed the experiments to focus on the underlying kinetics of the PCDTBT:PCBM photo-oxidation independent of lateral oxygen diffusion kinetics; it has previously been shown that for devices with an oxygen blocking top contact, lateral oxygen diffusion kinetics can extend over days.^{29,30} It is striking that only 10 minutes of light exposure result in an overall PCE loss of over 40%, due to simultaneous drops in short-circuit current density (*J*_{sc}), open-circuit voltage (*V*_{oc}) and fill factor (FF). After 60 minutes of exposure, a PCE loss of over 70% is seen. Devices exposed to air in the dark show similar performance to the fresh devices (Fig. S1 and Table S2, ESI†), indicating that the degradation process is driven by the combination of light and oxygen. The above experiments were repeated using interlayers of different polarity (MoO₃ and ZnO as well as PEDOT:PSS) underneath the active layer. The results (Fig. S2, ESI†) show a similar trend to the one in Fig. 1(a).

To identify the origin of device degradation and quantify the degradation products, ultraviolet-visible (UV-vis) spectroscopy, atomic force microscopy (AFM), X-ray photoelectron spectroscopy (XPS) and matrix-assisted laser desorption/ionization time-of-flight (MALDI-TOF) mass spectrometry measurements were carried out. Degraded blend films were fabricated and exposed in the same way as the films used for the devices in Fig. 1(a). No obvious photo-bleaching of the blend films was observed within the timescale studied (Fig. S3, ESI†). AFM images reveal minimal changes in surface morphology upon photo-oxidation (Fig. S4, ESI†). XPS measurements reveal a steady increase in bulk oxygen composition with increasing degradation time, and a concentration of oxidised species that is fairly uniform with depth below the surface layers (Fig. S5, ESI†). The samples for MALDI-TOF measurements were prepared by re-dissolving the blend films after photochemical degradation.

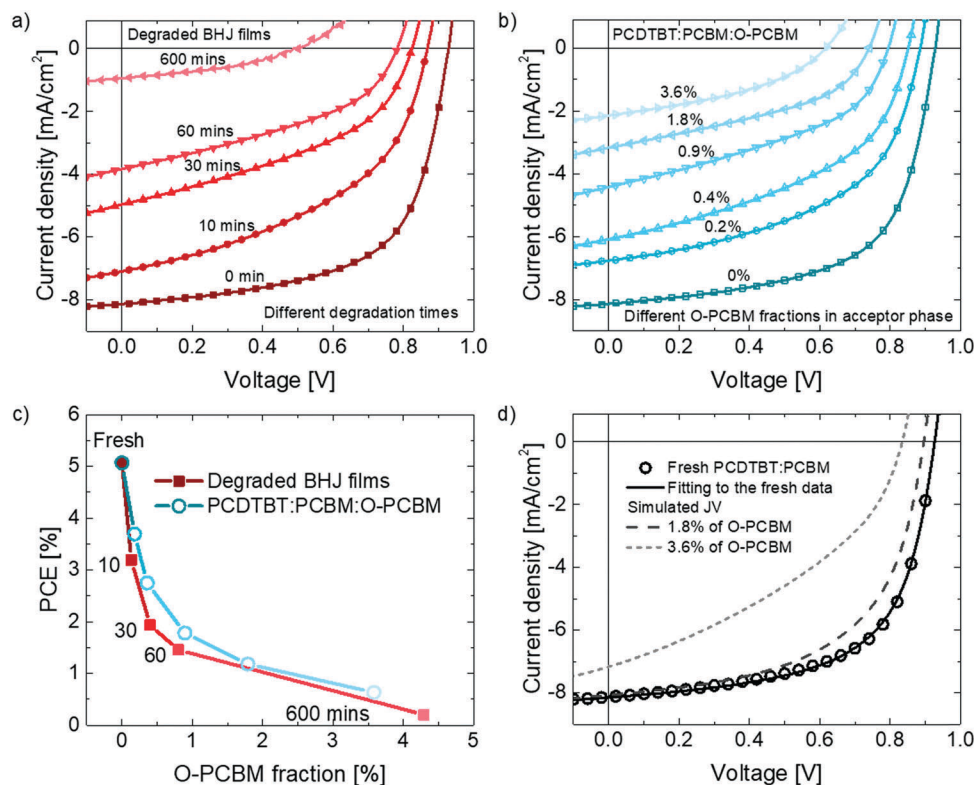


Fig. 1 Impact of fullerene photo-oxidation on OPV devices behaviour. (a) Current density–voltage (J – V) characteristic of ITO/PEDOT:PSS/PCDTBT:PCBM (1 : 2)/Ca/Al devices with different degradation times under simulated AM 1.5G illumination in air (the films were exposed to solar simulated light prior to back contact deposition); (b) J – V characteristic of PCDTBT:PCBM blend devices made with different fractions of degraded PCBM (the PCBM was degraded in solution prior to active layer processing), the percentages indicating the mass fraction of O-PCBM in the fullerene phase. All devices were encapsulated in nitrogen before characterisation. (c) PCE as a function of O-PCBM fraction for degraded PCDTBT:PCBM devices and pre-degraded PCBM devices; and (d) experimental (open circles) and simulated J – V characteristics for a device with pristine PCDTBT:PCBM (black); also simulated J – V characteristics for devices with increasing fraction of O-PCBM (dark grey dash line: 1.8% and light grey short dash line: 3.6%), reconstructed using the mobilities, trap energies and trap densities obtained from the space-charge-limited current analysis (see Fig. 3). Full device parameters are summarised in Tables S1 and S2 (ESI[†]).

By comparing Fig. 2(a) with (b) it is seen that photo-oxidised PCBM species (with up to 4 oxygen atoms) were formed upon 60 minutes of AM 1.5G exposure in air in the blend film with PCDTBT. The degree of oxidation is further increased with exposure duration (up to 7 oxygen atoms after 10 hours) as is seen in Fig. 2(c). An analysis of the ^{12}C -isotopic peak areas reveals a total of 0.8% oxidised PCBM in the blend film after 1 hour of aging. This is further increased to 4.3% after 10 hours of aging. The calculated quantity of photo-oxidised species is in good agreement with the bulk analysis of oxidised species by X-ray photoelectron spectroscopy (XPS) measurement. It thus appears that PCBM can be readily photo-oxidised upon exposure to light and oxygen of unprotected blend films of PCBM with conjugated donor polymers.

Although this study is focussed on the photostability of PCBM in particular, it is relevant to a number of other fullerene materials. As shown in Fig. S6 (ESI[†]), a similar photooxidation process leads to similar or higher concentration of oxidised fullerenes for other derivatives of C_{60} including the bis-adducts of PCBM and the indene derivative fullerene. The sensitivity of C_{60} derivatives to oxidation is consistent with the finding of Silva *et al.* that reactivity of fullerenes increases with reducing

pyramidalisation angle (*i.e.* with increasing curvature).³¹ In accordance with this we find a lower sensitivity of PC_{71}BM to the same oxidation procedure, indicating that whilst a variety of fullerene derivatives are readily oxidised, the chemical structure and shape of the fullerene influence its tendency to oxidise.

To isolate the impact of PCBM photo-oxidation alone (rather than degradation of the polymer) on the performance of OPV devices, we prepared blends of PCDTBT using PCBM that had been separately photo-oxidised in solution. Fig. 1(b) shows the current density–voltage characteristics of these devices (see also Table S3, ESI[†]). The aged PCBM species were also analysed by MALDI-TOF to estimate the fraction of oxidised PCBM as shown in Fig. 2(d). A PCBM solution exposed to AM 1.5G illumination in air for 72 hours contained 3.6% of oxidised PCBM (O-PCBM). Different amounts of degraded PCBM solution were mixed with a fresh PCBM solution to control the fraction of O-PCBM in the fullerene phase of blends with PCDTBT. The total concentration of fullerene (PCBM + O-PCBM) in the blend films was kept constant. XPS measurements of such films show uniform composition with depth, as expected (Fig. S5, ESI[†]). Markedly, with only 1% of oxidised PCBM in the fullerene phase a 65%

loss in device PCE was observed, which increased to $\sim 90\%$ loss with only 3.6% of O-PCBM. From this it is clear that the photo-oxidation of PCBM, even at low levels, has a significant impact on the performance of OPV devices. Fig. 1(c) compares the PCE of devices where the PCDTBT:PCBM films had been exposed to AM 1.5G illumination in air and PCDTBT:PCBM devices fabricated using different fractions of O-PCBM. Device PCEs are plotted against the fraction of O-PCBM in the active layer, measured by MALDI-TOF by removing and analysing the active layers. The drop in performance of photo-oxidised PCDTBT:PCBM blends quantitatively matches that of the devices made using O-PCBM. To investigate the generality of this effect, we extended our studies to other benchmark OPV systems, namely P3HT:PCBM, PTB7:PCBM, and PTB7-Th:PCBM blends, which exhibited qualitatively similar effects (Fig. S7, ESI†). It is thus apparent that PCBM photo-oxidation has a drastic impact on the performance of these benchmark OPV systems.

To establish the microscopic mechanism of device performance degradation, we explore the nature of the chemical defects formed upon photo-oxidation, and their effect on charge transport and recombination. As we demonstrate in the following, the insight provided by our study allows us to qualitatively reproduce the observed device behaviour under illumination as shown in Fig. 1(d), through simulations, by accounting for deteriorated electronic transport and increased recombination upon PCBM degradation.

Possible mechanisms of fullerene photo-oxidation

The effect of photo-oxidation on the highest occupied molecular orbital (HOMO) and lowest unoccupied molecular orbital

(LUMO) levels of PCBM was explored using electronic structure calculations of the products of oxidation, namely PCBM bearing epoxide, diol and carbonyl defects, following the oxidation mechanism reported by Xiao *et al.* as shown in Fig. 2(e).²¹ For each defect type, we identified all isomers with defects across 6–6 carbon bonds (*i.e.* two 6 membered rings together) and then calculated HOMO and LUMO energies as well as the total energy of the species using the delta self-consistent field (delta-SCF) method (see Methods section and Table S4, ESI†). Several oxidised species with multiple defects (*e.g.* two epoxides) and complex defect structures (*e.g.* two different defects) were included in the study for completeness. To check sensitivity of results to the calculation method, the HOMO and LUMO levels were also estimated using Kohn–Sham and time-dependent density functional theory (TD-DFT) methods (Tables S5 and S6, ESI†). For each method, the differences in HOMO and LUMO energies of any specific O-PCBM isomer relative to those of pristine PCBM were similar.

For each defect type, we calculated average HOMO and LUMO energies by including different isomers in proportion to their thermodynamic probability of occurrence, calculated from the total energy for the neutral species in a Boltzmann average (Table S7, ESI†). The oxidised PCBM species with the lowest total energy tend to have defects close to the phenyl butyric acid methyl ester side-chain; examples are shown by the molecular structures in Fig. 2(e). The LUMO is depressed for almost all oxidised PCBM species as shown in Fig. 2(e) (and Tables S4–S6 for full data set, ESI†), especially in the case of carbonyl defects. In contrast, the effect on the HOMO is small in all cases, except for the diol defect. Therefore, we expect the

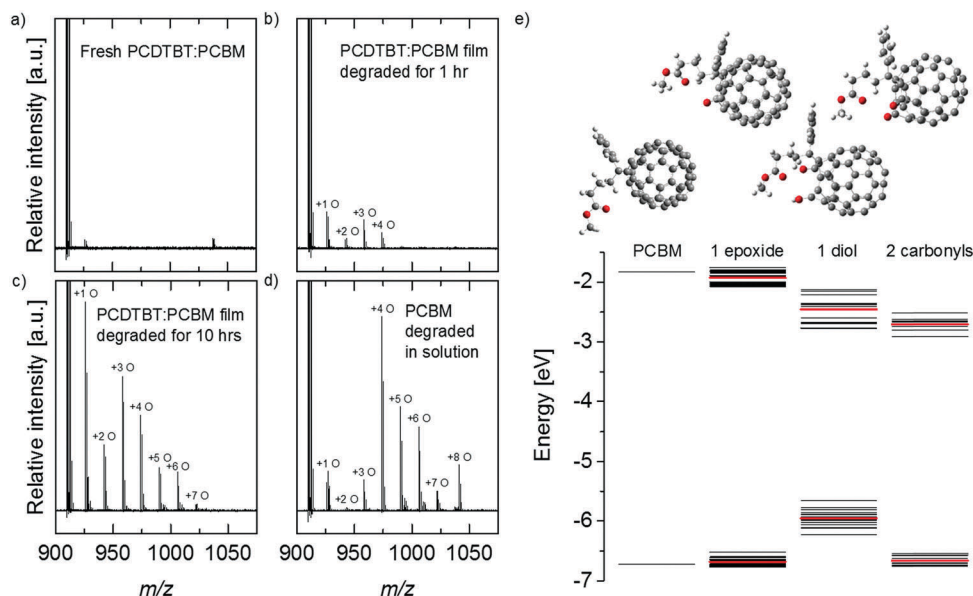


Fig. 2 Possible mechanisms of fullerene photo-oxidation. Negative ion mode MALDI-TOF measurement of (a) fresh PCDTBT:PCBM blend films; PCDTBT:PCBM blend films degraded under one sun in dry air for (b) 1 hour and (c) 10 hours; and (d) PCBM degraded in solution under one sun in dry air for 72 hours (see Fig. S8 for raw data, ESI†). (e) From left to right: HOMO and LUMO energies (calculated using a delta-SCF method) for neat PCBM, PCBM with one epoxide, PCBM with one diol and PCBM with two carbonyls defects. The different energies correspond to different possible positions of the defects on the fullerene cage. Boltzmann averages, based on total energy calculations, are given by the red lines. The molecular structures of PCBM, and an example of each defect type, are shown above their corresponding energy level diagram.

oxidation to affect electronic transport by introducing trap states for electrons, and to have a stronger effect on electron transport than on hole transport in the PCBM phase.

From Fig. 2(e) it is evident that, given the electron transport in a blend film takes place in the PCBM phase, the lower LUMO energies of the oxidised molecules will cause electron trapping. The distribution of electron trap states may be expected to extend deep (several tenths of an eV) into the band gap. The shape of the total density of trap states is difficult to predict, since the incidence of different defect types in practice is not known. However, the epoxide and carbonyl species would most likely give rise to both a broadening of the LUMO energies around an energy close to the LUMO of pristine PCBM as well as some deeper electron traps. Additionally, the overall density of defect states will increase with degradation.

Effects of fullerene oxidation on charge transport kinetics in neat PCBM films

To quantify the impact of photodegradation on electron transport we performed space-charge-limited current (SCLC) measurements on electron-only devices with structure (ITO/TiO₂/PCBM:O-PCBM/Ca/Al) made from PCBM solutions with different weight fractions of O-PCBM (0%, 0.2%, 0.9%, 1.8% and 3.6%). Effects of varying device thickness were minimised by comparing devices with approximately the same thickness of 70–80 nm. Representative current density–voltage curves in Fig. S9 (ESI[†]) show that the current density at a given applied voltage drops significantly with increasing fraction of photo-oxidised PCBM in the film. Also shown in Fig. S9 (ESI[†]) are calculated J – V curves obtained

by fitting the results of a drift-diffusion model that incorporates charge trapping to the experimental SCLC data.³² The model of the density of states (DoS) used for these fits consists of a narrow Gaussian distribution of N_t traps states per volume centred around an energy level lying E_t below the conduction band transport level, together with a band electron mobility, μ_0 .^{33,34} (Note that the band mobility represents the mobility of charge carriers at the transport level, in the absence of traps, rather than the effective mobility that would be measured.) The trap distribution is assumed constant with depth in accordance with the XPS measurements. Electrons are trapped and released by the sub-band-gap states according to a multiple-trapping model. Since only a single carrier type is present in SCLC measurements, recombination is negligible in these simulations. The parameters N_t , E_t , μ_0 and the electron injection barrier are varied to obtain the best fit for each device at each level of degradation (see Methods for further details). The model of a Gaussian distribution of traps was selected in preference to an exponential tail of states or a more complex DoS with multiple features because it provided the best fit to the data with the fewest fitting parameters. Fig. 3(a)–(c) show the obtained values of μ_0 , N_t and E_t , respectively for different fractions of O-PCBM using a large set of nominally identical devices in each case. Note that the range of fitted parameters increases with degradation, due to the microstructural variations inherent in the degradation process.

Fig. 3(a) shows that the band mobility obtained by this fitting drops by approximately one order of magnitude when the fraction of O-PCBM is increased from 0% to 3.6% (mobility values are

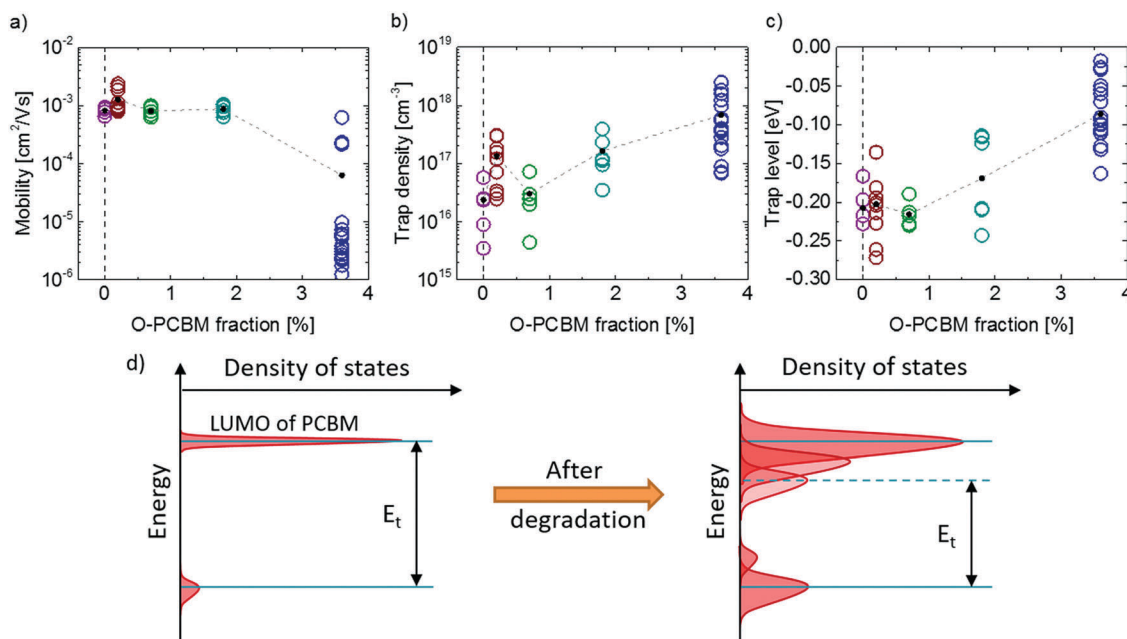


Fig. 3 Effects of fullerene oxidation on charge transport kinetics in neat PCBM films. Parameters obtained from analysis of space-charge-limited current measurements for PCBM electron-only devices with increasing fractions of O-PCBM: (a) electron “band” mobilities; (b) density of deep (Gaussian) traps; (c) depth of trap level below the LUMO of the pristine PCBM. (d) Schematic illustrating how the density of electron states may evolve during photo-oxidation. A number of repeated studies of fabrication and measurement were performed due to increasing variations of the band mobility, trap density and trap levels with increasing O-PCBM fraction caused by more severe film irregularity.

taken as the statistical average of a range of repeated runs of fabrication and measurement for each level of O-PCBM studied). At the same time, the density of traps increases by around an order of magnitude. For less degraded samples the trap level lies around 0.2 eV below the transport level of PCBM, while for higher O-PCBM concentrations the trap level and transport level are seen to approach each other as shown in Fig. 3(c), although the sample-to-sample variation in the extracted trap depth becomes large. The barrier for charge injection was found to be insensitive to degradation at around 0.3 eV (Fig. S9(f), ESI†). The SCLC results are consistent with the formation of both shallow and deep states below the LUMO of the PCBM, as expected from the quantum chemical calculations discussed in the previous section. The shallow states would serve both to push down the effective transport level and to reduce the 'band' mobility. This is illustrated schematically in Fig. 3(d).

By accounting for the data calculated in the SCLC analysis, we were able to reproduce the qualitative trend in current-voltage response under solar illumination of devices with increasing fraction of O-PCBM (Fig. 1d). We used the parameters obtained from SCLC for the DoS and band electron mobilities of the pristine, 1.8% degraded and 3.6% degraded films to represent the cases of fresh, partly and fully degraded films, respectively, and included band-to-band ($R_{\text{direct}} = 2.2 \times 10^{-20} \text{ m}^3 \text{ s}^{-1}$) and band-to-trap recombination, governed by the electron and hole densities along the capture and emission rate coefficients for electrons and holes (which were all set to the same value, $C_0^- = C_+^- = C_0^+ = C_+^+ = 10^{-16} \text{ m}^3 \text{ s}^{-1}$), as well as series and shunt resistances ($R_s = 4 \Omega \text{ cm}^2$ and $R_p = 1.9 \text{ k}\Omega \text{ cm}^2$, respectively). Our modelling strategy was to choose the recombination coefficients, parasitic resistances and hole mobility to best fit the J - V curve of the fresh device, and then modify only the parameters related to electron transport (*i.e.*, the electron band mobility, trap density and position of the electron transport level relative to the trap level) according to the values obtained from the SCLC analysis for different levels of degradation. In this way, we could reproduce the trend in current-voltage sweeps observed in the real devices, specifically, the losses in V_{oc} , J_{sc} and fill factor with increasing O-PCBM content. The effect of degradation modelled this way is less severe than that observed experimentally. This could arise either from the variation in the electronic effect of a given fraction of O-PCBM (evident from the scatter in SCLC device behaviour at high levels of degradation) or from neglecting the impact of O-PCBM on another, secondary quantity, for example on hole mobility. Nevertheless, the qualitative reproduction of the trend in all parameters corroborates the link between traps and device performance.

Effects of fullerene oxidation on blend film recombination and transport kinetics

In order to further understand the effect of fullerene oxidation on device performance, particularly on V_{oc} , charge-carrier densities and lifetimes were measured by transient photocurrent (TPC), transient photovoltage (TPV) and charge-extraction (CE) measurements. The measured charge-carrier density at open

circuit, as a function of device V_{oc} under increasing illumination intensity, is plotted in Fig. 4(a). Fig. 4(b) shows the charge-carrier lifetimes measured as a function of these charge-carrier densities, under the same illumination conditions. As it can be observed in Fig. 4(a), in all devices the charge density rises approximately exponentially with V_{oc} , consistent with the presence of a tail of states in the band gap. We also note that these density of states curves are shifted substantially to lower energy with increasing fraction of O-PCBM: for a given charge-carrier density of $4.3 \times 10^{16} \text{ cm}^{-3}$, for example, the energetic differences are $\cong 140 \text{ mV}$ between the devices with 0% and 0.4% O-PCBM, and $\cong 130 \text{ mV}$ between those with 0.4% and 1% O-PCBM. Therefore, in order to achieve the same electron quasi-Fermi level position and therefore the same V_{oc} , much more charge has to be injected in the devices with O-PCBM, due to the deeper distribution of states within the band gap. Fig. 4(d) shows, for comparison, the charge-carrier density – V_{oc} behaviour expected for the DoS parameters for differently degraded devices obtained by modelling the devices with the same set of parameters obtained from SCLC analysis and used to model the J - V curves in Fig. 1(d) above. The approximately exponential form of the $n(V_{\text{oc}})$ curves and the shift to lower V_{oc} with degradation are reproduced, supporting the idea that the changes in transport and density of states both arise from the introduction of electron trap states.

Fig. 4(b) shows that the devices with higher O-PCBM fractions exhibit longer charge lifetimes at fixed charge density. Longer charge-carrier lifetimes are consistent with increased trapping in localized states, which can slow down recombination at a given charge density by reducing the rate at which charge carriers meet. The V_{oc} values calculated from these two opposing effects, *i.e.* longer lifetimes and higher density of sub-gap states with increasing O-PCBM fraction, match the measured V_{oc} values at varying illumination intensity as shown in Fig. 4(c) (see ESI† for the mathematical background), consistent with this analysis. The introduction of electron trap states results in slower recombination at fixed charge density but that does not benefit V_{oc} because a higher charge density (which leads to faster recombination) is needed to achieve the same quasi-Fermi level separation.

TPV measurements provide information on the total recombination in a device, but cannot discriminate between different mechanisms, such as band-to-band, trap mediated or surface recombination. A first indication of the dominant recombination mechanism comes from the ideality factors measured from the dependence of V_{oc} on light intensity [Fig. 4(c)]. The ideality factors are related to the reaction order of recombination such that n_{id} tends to increase from $\cong 1$ to $\cong 2$ either when recombination becomes stronger in the bulk of the active layer compared to its interfaces with the electrodes, or when the recombination involves deeper trap states in the band gap.³⁵ Here, the increase in n_{id} with O-PCBM fraction indicates that the recombination mechanism changes with increasing oxidation. Both scenarios (more bulk traps and deeper traps) are consistent with the n_{id} behaviour. The same trends found in devices containing O-PCBM were found in devices prepared from blends degraded as films, as seen in Fig. S10 (ESI†),

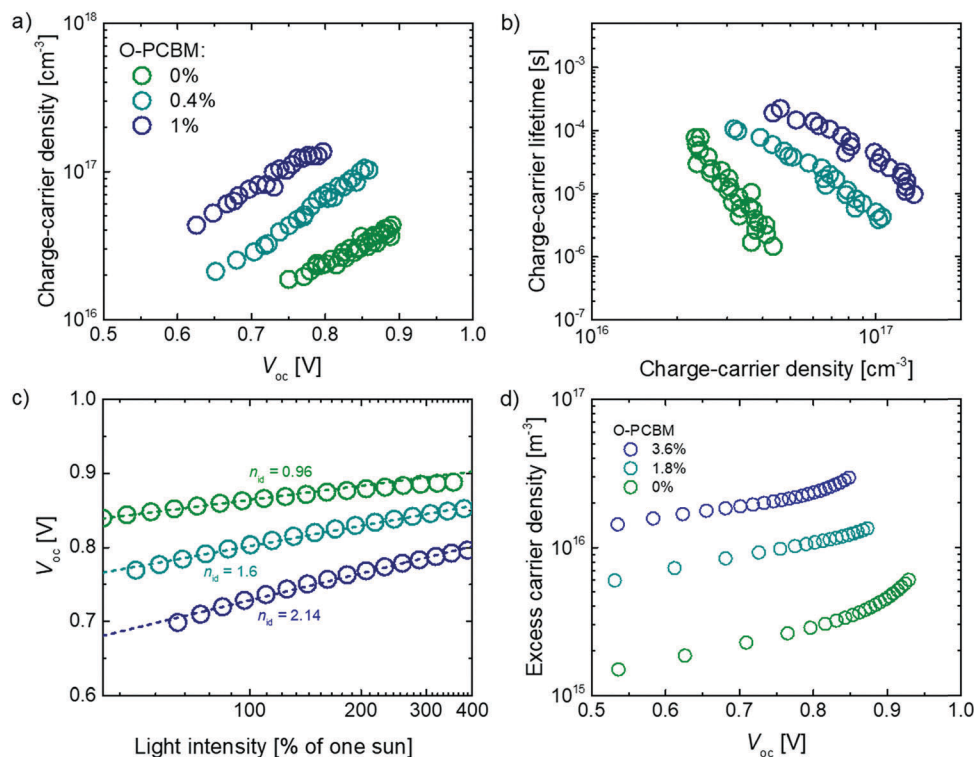


Fig. 4 Effects of fullerene oxidation on blend film recombination and transport kinetics. CE, TPV and TPC analysis of PCDTBT:PCBM devices with increasing fraction of O-PCBM: (a) charge-carrier density at varying V_{oc} (produced by varying the illumination intensity); (b) charge-carrier lifetimes at varying charge-carrier density [calculated from (a)]; (c) measured V_{oc} (open circles) at varying illumination intensities (the dashed lines indicate linear fits to the data); (d) simulated charge carrier density versus V_{oc} for different levels of degradation. Note that the devices under study exhibited high shunt currents under low illumination conditions (below 0.3 Sun), and therefore those data were not included in the analysis.

eliminating electrode degradation as the cause of the change in TPV behaviour.

Finally, charge-extraction measurements carried out at short circuit (rather than at open circuit as above), allow us to assay the average (combining electron and hole) charge-carrier mobility in the OPV devices. The mobility inferred from these charge extraction data decreased with increasing fraction of O-PCBM (Fig. S11, ESI†), consistent with increased carrier trapping and in qualitative agreement with the SCLC data discussed above. The magnitude of the reduction of mobility upon degradation is lower than obtained by SCLC, however the mobility estimated from charge extraction includes hole mobility, which should be less affected by fullerene oxidation.

Electroluminescence analysis of the effect of fullerene photooxidation on voltage losses

As a complementary probe of the effect of degradation on blend DoS we characterised the series of PCDTBT:(PCBM:O-PCBM) devices using electroluminescence (EL) and sub-band gap external quantum efficiency (EQE) measurements. Shown in Fig. 5a are normalised EL spectra for fresh and degraded devices. The peak at ≈ 1.2 eV is assigned to radiative decay of the charge-transfer state at the PCDTBT:PCBM interface, in agreement with previous measurements.³⁶ Control experiments on pure PCDTBT or PCBM confirmed that the emission did not arise from band-to-band recombination from either species (Fig. S12, ESI†). The emission

of the charge-transfer state is shifted to slightly lower energies in samples containing increasing fractions of O-PCBM, and its quantum yield decreases (higher injection current is required to obtain a detectable emission). The lower emission efficiency observed in devices with oxidised PCBM is consistent with both poorer transport and a higher degree of non-radiative recombination compared to radiative recombination.

Also shown in Fig. 5(a) are sub-band gap EQE spectra, obtained by combining measured EQE with the measured EL spectra, using a detailed balance approach (for devices containing other fractions of O-PCBM see Fig. S13, ESI†).³⁷ The presence of an increasing fraction of charge-transfer states with lower energy than in fresh blends is evident from the decreasing slope of the sub-band-gap EQE curves, which indicates that the contribution to EQE of the sub-band-gap density of states becomes more pronounced with increasing O-PCBM fraction.

From the sub-band-gap EQE data we were able to calculate the V_{oc} that could theoretically be obtained if the only loss mechanism was radiative recombination ($V_{oc,rad}$) following a previously reported approach.³⁷ This value is normally lower than the V_{oc} in the Shockley–Queisser limit for single junction solar cells because of the non-step-like absorption profile of practical devices such as these. The difference between the resulting radiative-limit $V_{oc,rad}$ and the measured V_{oc} can be assigned to non-radiative recombination losses ($\Delta V_{oc,non-rad}$). Shown in Fig. 5(b) are the contributions to V_{oc} losses. The relative

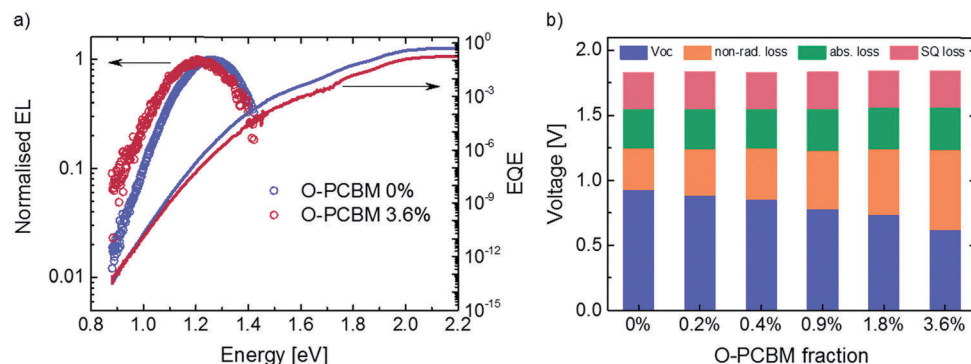


Fig. 5 Electroluminescence analysis of the effect of fullerene photooxidation on voltage losses. (a) EL and sub-band gap EQE data for PCDTBT:PCBM with 0% and 3.6% O-PCBM (the data for intermediate concentrations were omitted for clarity; full dataset available in the ESI†); the EQE data for energies below ~ 1.25 eV was calculated from the EL data (b) experimental V_{oc} compared to ideal V_{oc} for devices without non-radiative recombination ($V_{oc,rad}$), and according to the Shockley–Queisser limit ($V_{oc,SQ}$) and the band gap of the polymer (E_g/q).

size of the $\Delta V_{oc,non-rad}$ component for different devices in a series should reflect the degree of non-radiative recombination, as described above, for devices with different fractions of O-PCBM. The losses due to non-radiative recombination clearly increase with increasing fraction of O-PCBM, consistent with the formation of sub-band gap trap states that slow down carrier collection and increase the overall likelihood of non-radiative recombination. (See Table S8 for all the V_{oc} values, ESI†) These results are in good agreement with the clear increase in trap-mediated recombination inferred from the ideality factors (Fig. 4(c)).

Discussion

Environmental stability has become a primary concern for the realisation of low-cost manufacture of opto-electronic devices using approaches that typically involve air processing and minimal encapsulation. Despite the significant amount of research effort, the origin of the limited environmental stability of devices such as polymer:fullerene solar cells remains unclear. It is recognised that different stress factors (oxygen, water, heat) are involved and that different components of the device are vulnerable (semiconductors, interlayers electrodes) but few studies unambiguously relate particular chemical degradation mechanisms to their impact on electrical performance. Whilst substantial research efforts have addressed the photochemical and photophysical stability of conjugated donor polymers,^{5,6,8,38} the environmental stability of fullerenes and their impact on device performance have received relatively little attention.^{22–25} A further consideration is that in most studies to date the chemical nature of defects is not identified and so the precise relationship between degradation mechanism and device behaviour cannot be explored. Here, we used a systematic study of the impact of fullerene oxidation on solar cell performance to demonstrate that common products of the photo-oxidation of PCBM, specifically fullerene epoxides and carbonyls, act as electron traps in OPV devices. Whilst prior studies had shown that epoxides²⁷ and other oxygenic defects^{21,31} were expected to form on fullerenes, and that in practice oxygen exposure changes the electronic structure of

fullerenes²² with impact on device performance,²³ the link between chemical nature of such defects and electrical properties of devices had not previously been investigated. Previous approaches to simulate the effect of degradation have typically addressed the effect on photocurrent collection of oxidative p-doping of the active layer,^{39,40} or invoked trap states to explain changes in electrical response,^{41–43} but without a clear origin for those defects. In this work, we have established a quantitative relationship between the presence of specific oxidative defects which act as electron traps and the resulting change in electronic properties of the OPV devices made from the oxidised fullerene, which has not been established previously. Specifically, electron mobility, charge lifetime and density of states measurements are all consistent with the presence of a distribution of electron trap states centred around 0.2 eV below the conduction band edge, which increases with fraction of oxidised fullerene. Shallow traps in this energy range have been previously observed in PCBM without any intentional degradation.⁴⁴ By using a device model to account for the effect of these trap states on charge carrier densities, electron transport and recombination, we could show how the introduction of oxidised PCBM causes losses in device open-circuit voltage, short-circuit current and fill factor. More generally, this study demonstrates, at least for similar systems, that when the chemical mechanism of degradation, or the degradation products, are known, we can, in principle, predict the consequences for electronic processes.

Interestingly, we have found that even exposure to low light conditions, typical of laboratory environments, is sufficient to drive the photo-oxidation of fullerenes in polymer:fullerene solar cells, corroborating previous studies on fullerene films (Fig. S1, ESI†).²² This observation suggests that inadvertent exposure to light and oxygen during sample preparation and characterisation (*e.g.* optical measurements) is as problematic as illumination of the device under operation. Finally, the results reported herein suggest that PCBM, one of the most commonly used fullerene derivatives in the community to date, may not be an ideal candidate for the commercialisation of stable opto-electronic devices due to their intrinsic instability. Alternative small-molecular acceptor materials, which do not

undergo epoxide formation so readily as fullerenes, could be good candidates to extend the lifetime of organic solar cells. Preliminary studies suggest that photodegradation is slower using some non-fullerene acceptors,⁴ but more detailed studies are needed. Our findings thus highlight the importance of developing alternative electron accepting/transporting materials with improved photochemical stability. Our findings are also relevant for stability of perovskite devices, where PCBM is commonly used as an electron collecting interlayer.⁴⁵

It should be re-iterated that the degradation of organic solar cells results from the interplay of multiple concurrent pathways, typically induced by different environmental stress factors. In order to achieve overall environmental stability of organic solar cells, all of these degradation mechanisms need to be identified and addressed. For example, it has been demonstrated that some donor polymers may act as suppressing agents to fullerene oxidation,²⁰ likely owing to their low oxygen solubility and short triplet lifetime.^{14,46} While the work presented here demonstrates the important role of fullerenes in the environmental stability of organic solar cells, the development of environmentally stable donor materials, interlayers and electrodes are of equal importance in addressing the stability challenge of organic electronic devices.

Methods

Materials

PCDTBT was purchased from 1-materials. All fullerene were purchased from Solenne BV. Chlorobenzene (CB), zinc acetate dihydrate, 2-methoxyethanol, and ethanolamine were purchased from Sigma Aldrich. MoO₃ was purchased from Strem Chemicals. All materials were used as received.

Device fabrication

ITO glass substrates were cleaned sequentially with Hellmanex detergent, deionized water, acetone, and isopropyl alcohol in ultrasonic bath. Poly(3,4-ethylenedioxythiophene)-poly(styrene-sulfonate), Heraeus Clevis P VP AI 4083, (PEDOT:PSS) or ZnO precursor solution (109.8 mg of zinc acetate dihydrate dissolved in 1 mL of 2-methoxyethanol and 30.2 μ L of ethanolamine) was spin-coated on plasma treated ITO substrates at 4000 rpm for 40 s, followed by thermal annealing at 150 °C for 10 minutes. For the devices using MoO₃ as the interlayer, 10 nm of MoO₃ was thermally evaporated on the ITO coated glasses under vacuum of 2×10^{-5} mbar. PCDTBT and PCBM (1:2) were co-dissolved in CB at 60 °C and stirred at 1300 rpm with a total concentration of 18 mg mL⁻¹ for over 12 hours in nitrogen filled glovebox. The blend solution was spin-coated on PEDOT:PSS, MoO₃, or ZnO coated substrates in air, resulting in active layers with a thickness of \sim 70 nm. Finally, 30 nm of calcium and 100 nm of aluminium (or 10 nm of MoO₃ and 100 nm of silver for ZnO device) were thermally evaporated on the blend layer under vacuum of 2×10^{-5} mbar, defining active area of 0.15 cm². The devices were encapsulated by glass slides using epoxy in nitrogen filled glovebox prior to measurement. Current density-voltage (J - V)

characterizations were performed by a Keithley 2400 source-meter under AM 1.5G illumination, Newport 92193A-1000 solar simulator with a light intensity of 90 mW cm⁻².

Degradation

PCDTBT:PCBM films fabricated on PEDOT:PSS coated ITO glass substrates were degraded under AM 1.5G illumination in dry air (relative humidity \sim 30%) for different periods of time mentioned in the main text. PCBM solution for selective degradation study was prepared by dissolving PCBM (24 mg) in CB (1 mL) in a 15 mL vial at 60 °C with stir speed of 1300 rpm in a nitrogen filled glovebox for at least 12 hours. The vial of PCBM solution was then filled with air and degraded under AM 1.5G illumination with stir speed of 300 rpm for 72 hours in air.

XPS measurements

XPS data were obtained using a Kratos Axis Supra (Kratos Analytical, Manchester, UK) using a monochromated Al K α source. All spectra were recorded using a charge neutralizer to limit differential charging. The main carbon peak is charge referenced to 284.5 eV.^{47,48} Depth profiles of different samples were generated by rastering a 2.5 kV Ar₅₀₀⁺ cluster beam over a 3 mm \times 3 mm area giving a typical sample current of 5.53 nA. The data was fitted using CASA XPS with Shirley backgrounds.

MALDI-TOF measurements

All samples were dissolved in chlorobenzene at an approximate concentration of 1 mg mL⁻¹. MALDI matrix *trans*-2-[3-(4-*tert*-butylphenyl)-2-methyl-2-propenylidene]malononitrile (DCTB) was purchased from Insight Biotechnology Ltd (Wembley, UK), and dissolved in chlorobenzene at 20 mg mL⁻¹. Solutions of sample and matrix were mixed together so the matrix is in \sim 250–1000 fold molar excess, typically 1 μ L of sample to 49 μ L of matrix. 0.5 μ L of each of these mixture solutions for each sample was spotted onto the MALDI plate and dried in air. MALDI-TOF spectra were acquired in negative-reflectron mode using an ultrafleXtreme mass spectrometer (Bruker Daltonics, Bremen, Germany), which is equipped with a Smartbeam-II Nd:YAG laser (λ = 355 nm). Data was acquired using flexControl software v3.4, while post-acquisition processing of data was performed by flexAnalysis software v3.4. PCBM and oxidised analogues were observed as negative radical ion species ($M^{\bullet-}$). The percentage of photo-oxidised fullerenes was determined by calculating the peak areas of the oxidised fullerene species.

DFT calculations

We performed single point energy calculations on optimised structures in Gaussian09 for N , $N + 1$ and $N - 1$ electron systems. The HOMO (and LUMO) levels are then found by computing the difference between total energy for the N electron system with the $N - 1$ ($N + 1$) system. All calculations were done at the B3LYP level of theory with the 6-31g* basis set.⁴⁹

Electroluminescence

EL was measured using a spectrograph (Andor Shamrock 303) combined with a InGaAs photodiode array (Andor iDUS 491)

cooled to -90°C , calibrated with a Bentham CL2 quartz halogen lamp with known emission spectrum. EL spectra were collected at injection current densities up to 100 mA cm^{-2} , on at least 4 devices for each fraction of O-PCBM.

External quantum efficiency

EQE was measured using a grating spectrometer (CVI DIGIKROM 240) to create monochromatic light combined with a tungsten halogen light source. The monochromatic light was modulated at 290 Hz with a chopper, and a Stanford Research Systems SR380 lock-in amplifier, with an internal transimpedance amplifier of 106 V A^{-1} , was used to detect the photocurrent. Long pass filters at 780 and 850 nm were used to filter out the scattered light from the monochromator. The spectra were taken from 300 to 1000 nm and calibrated by a silicon photodiode.

Electron only devices

Glass substrates containing a predefined layer ($\approx 70\text{ nm}$) of indium doped tin oxide (ITO) were ultrasonicated in an acetone bath, and subsequently in an IPA bath, for 10 minutes, respectively. The substrates were dried using nitrogen. Titanium dioxide (TiO_2) films were deposited onto the ITO by spin coating of a precursor solution containing $70\text{ }\mu\text{L}$ titanium isopropoxide, $55\text{ }\mu\text{L}$ ethanol-amine and 1 mL 2-methoxyethanol. The substrates were sintered in an oven for 1 hour at 500°C . The resulting TiO_2 film is approximately 20 nm thick. The pre-degraded PCBM was spun onto the substrates with a target film thickness of around 80 nm . The back contact was applied by thermal annealing under high vacuum ($<5 \times 10^{-6}\text{ Torr}$). Calcium (Ca) was evaporated at a rate $1\text{ }\text{\AA s}^{-1}$ with a final thickness of around 30 nm . A thick layer of aluminium was subsequently evaporated at a rate of $20\text{ }\text{\AA s}^{-1}$ with a resulting layer thickness of 150 nm . The resulting electron-only device had the following device architecture: glass/ITO/ TiO_2 /PCBM/Ca/Al. The devices were stored and measured under inert atmosphere (N_2) and in the dark.

SCLC measurements

The current density–voltage (J - V) curves were recorded using a source measurement unit (SMU) using a slow scan rate to ensure that the device was in a steady-state condition. J - V curves were recorded in both forward ($0 \rightarrow 5\text{ V}$) and in reverse ($0 \rightarrow -5\text{ V}$) bias. Since no difference in the magnitude or the shape of the current was observed irrespective of bias polarity, the presence of built-in voltages across the device can be ruled out. The J - V curves were analysed using a commercially available drift-diffusion solver called Advanced Semiconductor Analysis (ASA). The software uses a multiple trapping-release model which assumes that all charge carriers must be released from charge traps to the transport level in order to contribute to the current. Traps were modelled using a Gaussian distribution of states below the conduction band edge, where we allowed for the Gaussian density and the trap level to vary while the Gaussian standard deviation was set to 0.1 eV . To fit the experimental J - V curves with the model we allowed the trap density, trap depth, electron band mobility and barrier for electron injection to vary simultaneously.

Author contributions

Device fabrication and stability studies were carried out by H. K. H. L. and Z. L. MALDI-TOF measurements were carried out by M. F. W. AFM measurements were carried out by J. R. S. and XPS depth profiles by J. M. DFT calculations were performed by B. R. EL measurements were performed by A. M. T., and sub-band gap EQE measurements were carried out by S. M. T. and A. D. C. M. SCLC measurements and J - V simulations were carried out by J. A. R. TPV and CE measurements were carried out by J. W. J. M., T. W., E. S. and S. P. contributed to sample preparation and device fabrication. H. K. H. L., J. R. D., A. M. T., T. K. and W. C. T. contributed to project planning and discussions. Z. L. and J. N. had the idea, led the project, and prepared the manuscript. All authors contributed to the manuscript preparation.

Conflicts of interest

The authors declare no competing financial interests.

Acknowledgements

The authors would like to acknowledge the funding support from the Welsh Assembly Government funded Sêr Cymru Solar Project, and the National Research Network in Advanced Engineering and Materials, the European Commission's CHEETAH Project (FP7-Energy-2013 – Grant no. 609788) and EPSRC grants EP/M025020/1 and EP/K030671/1. ZL thanks the Welsh Assembly Government Sêr Cymru II fellowship scheme, AMT thanks the Imperial College Junior Research Fellowship scheme, ADCM thanks CNPq-Brazil PDE fellowship (Grant 207507/2014-7), JAR thanks the EPSRC Doctoral Training Centre in Plastic Electronics (EP/G037515/1) and BR thanks the EPSRC Doctoral Training Centre in Theory and Simulation of Materials (EP/G036888/1) for funding.

References

- 1 Y. Cui, *et al.*, Fine-Tuned Photoactive and Interconnection Layers for Achieving over 13% Efficiency in a Fullerene-Free Tandem Organic Solar Cell, *J. Am. Chem. Soc.*, 2017, **139**, 7302–7309.
- 2 Y. Liu, *et al.*, Aggregation and morphology control enables multiple cases of high-efficiency polymer solar cells, *Nat. Commun.*, 2014, **5**, 5293, DOI: 10.1038/ncomms6293.
- 3 W. Zhao, *et al.*, Fullerene-Free Polymer Solar Cells with over 11% Efficiency and Excellent Thermal Stability, *Adv. Mater.*, 2016, **28**, 4734–4739, DOI: 10.1002/adma.201600281.
- 4 D. Baran, *et al.*, Reducing the efficiency-stability-cost gap of organic photovoltaics with highly efficient and stable small molecule acceptor ternary solar cells, *Nat. Mater.*, 2017, **16**, 363–369.
- 5 M. Jørgensen, K. Norrman and F. C. Krebs, Stability/degradation of polymer solar cells, *Sol. Energy Mater. Sol. Cells*, 2008, **92**, 686–714.
- 6 M. Jørgensen, *et al.*, Stability of Polymer Solar Cells, *Adv. Mater.*, 2012, **24**, 580–612.

- 7 C. J. M. Emmott, *et al.*, *In situ*, long-term operational stability of organic photovoltaics for off-grid applications in Africa, *Sol. Energy Mater. Sol. Cells*, 2016, **149**, 284–293.
- 8 K. Kawano, *et al.*, Degradation of organic solar cells due to air exposure, *Sol. Energy Mater. Sol. Cells*, 2006, **90**, 3520–3530, DOI: 10.1016/j.solmat.2006.06.041.
- 9 R. Ahmed, C. Simbrunner, G. Schwabegger, M. A. Baig and H. Sitter, Air stability of C60 based n-type OFETs, *Synth. Met.*, 2014, **188**, 136–139.
- 10 T. Heumueller, *et al.*, Morphological and electrical control of fullerene dimerization determines organic photovoltaic stability, *Energy Environ. Sci.*, 2016, **9**, 247–256, DOI: 10.1039/C5EE02912K.
- 11 T. Heumueller, *et al.*, Reducing burn-in voltage loss in polymer solar cells by increasing the polymer crystallinity, *Energy Environ. Sci.*, 2014, **7**, 2974–2980, DOI: 10.1039/C4EE01842G.
- 12 Z. Li, *et al.*, Performance enhancement of fullerene-based solar cells by light processing, *Nat. Commun.*, 2013, **4**, 2227.
- 13 S. Wood, *et al.*, Natures of optical absorption transitions and excitation energy dependent photostability of diketopyrrolopyrrole (DPP)-based photovoltaic copolymers, *Energy Environ. Sci.*, 2015, **8**, 3222–3232, DOI: 10.1039/C5EE01974E.
- 14 Y. W. Soon, *et al.*, Correlating triplet yield, singlet oxygen generation and photochemical stability in polymer/fullerene blend films, *Chem. Commun.*, 2013, **49**, 1291–1293, DOI: 10.1039/c2cc38243a.
- 15 A. Distler, *et al.*, Effect of PCBM on the Photodegradation Kinetics of Polymers for Organic Photovoltaics, *Chem. Mater.*, 2012, **24**, 4397–4405.
- 16 A. M. Rao, *et al.*, Photoinduced Polymerization of Solid C₆₀ Films, *Science*, 1993, **259**, 955–957.
- 17 P. C. Eklund, A. M. Rao, P. Zhou, Y. Wang and J. M. Holden, Photochemical transformation of C₆₀ and C₇₀ films, *Thin Solid Films*, 1995, **257**, 185–203.
- 18 A. Distler, *et al.*, The Effect of PCBM Dimerization on the Performance of Bulk Heterojunction Solar Cells, *Adv. Energy Mater.*, 2014, **4**, 1300693.
- 19 F. Piersimoni, *et al.*, Influence of fullerene photodimerization on the PCBM crystallization in polymer:fullerene bulk heterojunctions under thermal stress, *J. Polym. Sci., Part B: Polym. Phys.*, 2013, **51**, 1209–1214.
- 20 Y. Shogo, *et al.*, MALDI-TOF MS Study of the Photooxidation of PCBM and Its Suppression by P3HT, *Chem. Lett.*, 2015, **44**, 339–341, DOI: 10.1246/cl.141025.
- 21 Z. Xiao, *et al.*, Synthesis of [59]Fullerenones through Peroxide-Mediated Stepwise Cleavage of Fullerene Skeleton Bonds and X-ray Structures of Their Water-Encapsulated Open-Cage Complexes, *J. Am. Chem. Soc.*, 2007, **129**, 16149–16162.
- 22 A. S. Anselmo, A. Dzwilewski, K. Svensson and E. Moons, Photodegradation of the electronic structure of PCBM and C60 films in air, *Chem. Phys. Lett.*, 2016, **652**, 220–224.
- 23 R. Hansson, *et al.*, Photo-degradation in air of the active layer components in a thiophene-quinoxaline copolymer:fullerene solar cell, *Phys. Chem. Chem. Phys.*, 2016, **18**, 11132–11138.
- 24 S. Yamane, *et al.*, Photooxidation studies on indene-C60 adducts, *Sol. Energy Mater. Sol. Cells*, 2015, **143**, 135–140.
- 25 Y. Matsuo, *et al.*, Deterioration of bulk heterojunction organic photovoltaic devices by a minute amount of oxidized fullerene, *Chem. Commun.*, 2012, **48**, 3878–3880.
- 26 G. Volonakis, L. Tsetseris and S. Logothetidis, Impurity-related degradation in a prototype organic photovoltaic material: a first-principles study, *Org. Electron.*, 2013, **14**, 1242–1248.
- 27 M. O. Reese, *et al.*, Photoinduced Degradation of Polymer and Polymer–Fullerene Active Layers: Experiment and Theory, *Adv. Funct. Mater.*, 2010, **20**, 3476–3483.
- 28 C. H. Peters, *et al.*, High Efficiency Polymer Solar Cells with Long Operating Lifetimes, *Adv. Energy Mater.*, 2011, **1**, 491–494, DOI: 10.1002/aenm.201100138.
- 29 T. Jeranko, H. Tributsch, N. S. Sariciftci and J. C. Hummelen, Patterns of efficiency and degradation of composite polymer solar cells, *Sol. Energy Mater. Sol. Cells*, 2004, **83**, 247–262.
- 30 S. Shoaee and J. R. Durrant, Oxygen diffusion dynamics in organic semiconductor films, *J. Mater. Chem. C*, 2015, **3**, 10079–10084.
- 31 H. S. Silva, J. Cresson, A. Rivaton, D. Bégue and R. C. Hiorns, Correlating geometry of multidimensional carbon allotropes molecules and stability, *Org. Electron.*, 2015, **26**, 395–399.
- 32 M. Zeman and J. Krc, Optical and electrical modeling of thin-film silicon solar cells, *J. Mater. Res.*, 2008, **23**, 889–898.
- 33 J. Dacuna and A. Salleo, Modeling space-charge-limited currents in organic semiconductors: extracting trap density and mobility, *Phys. Rev. B: Condens. Matter Mater. Phys.*, 2011, **84**, 195209.
- 34 H. T. Nicolai, M. M. Mandoc and P. W. M. Blom, Electron traps in semiconducting polymers: exponential versus Gaussian trap distribution, *Phys. Rev. B: Condens. Matter Mater. Phys.*, 2011, **83**, 195204.
- 35 T. Kirchartz, F. Deledalle, P. S. Tuladhar, J. R. Durrant and J. Nelson, On the Differences between Dark and Light Ideality Factor in Polymer:Fullerene Solar Cells, *J. Phys. Chem. Lett.*, 2013, **4**, 2371–2376.
- 36 M. A. Faist, *et al.*, Competition between the Charge Transfer State and the Singlet States of Donor or Acceptor Limiting the Efficiency in Polymer:Fullerene Solar Cells, *J. Am. Chem. Soc.*, 2012, **134**, 685–692, DOI: 10.1021/ja210029w.
- 37 J. Yao, *et al.*, Quantifying Losses in Open-Circuit Voltage in Solution-Processable Solar Cells, *Phys. Rev. Appl.*, 2015, **4**, 014020.
- 38 H. T. Nicolai, *et al.*, Unification of trap-limited electron transport in semiconducting polymers, *Nat. Mater.*, 2012, **11**, 882–887.
- 39 A. Seemann, *et al.*, Reversible and irreversible degradation of organic solar cell performance by oxygen, *Sol. Energy*, 2011, **85**, 1238–1249.
- 40 J. Schafferhans, A. Baumann, A. Wagenpfahl, C. Deibel and V. Dyakonov, Oxygen doping of P3HT:PCBM blends: influence on trap states, charge carrier mobility and solar cell performance, *Org. Electron.*, 2010, **11**, 1693–1700.
- 41 S. Khelifi, *et al.*, Investigation of defects by admittance spectroscopy measurements in poly(3-hexylthiophene):(6,6)-phenyl C₆₁-butyric acid methyl ester organic solar cells degraded under air exposure, *J. Appl. Phys.*, 2011, **110**, 094509.

- 42 M. Lenes, *et al.*, Electron Trapping in Higher Adduct Fullerene-Based Solar Cells, *Adv. Funct. Mater.*, 2009, **19**, 3002–3007.
- 43 R. Pacios, *et al.*, Effects of Photo-oxidation on the Performance of Poly[2-methoxy-5-(3',7'-dimethyloctyloxy)-1,4-phenylene vinylene]:[6,6]-Phenyl C₆₁-Butyric Acid Methyl Ester Solar Cells, *Adv. Funct. Mater.*, 2006, **16**, 2117–2126.
- 44 J. Schafferhans, C. Deibel and V. Dyakonov, Electronic Trap States in Methanofullerenes, *Adv. Energy Mater.*, 2011, **1**, 655–660.
- 45 J.-P. Correa-Baena, *et al.*, The rapid evolution of highly efficient perovskite solar cells, *Energy Environ. Sci.*, 2017, **10**, 710–727.
- 46 Y. W. Soon, *et al.*, Material Crystallinity as a Determinant of Triplet Dynamics and Oxygen Quenching in Donor Polymers for Organic Photovoltaic Devices, *Adv. Funct. Mater.*, 2013, **24**, 1474–1482, DOI: 10.1002/adfm.201302612.
- 47 M. H. Richter, D. Friedrich and D. Schmeißer, Valence and Conduction Band States of PCBM as Probed by Photoelectron Spectroscopy at Resonant Excitation, *J. Bionanosci.*, 2012, **2**, 59–65, DOI: 10.1007/s12668-011-0034-1.
- 48 J. Díaz, G. Paolicelli, S. Ferrer and F. Comin, Separation of the sp³ and sp² components in the C 1s photoemission spectra of amorphous carbon films, *Phys. Rev. B: Condens. Matter Mater. Phys.*, 1996, **54**, 8064–8069.
- 49 R. O. Jones and O. Gunnarsson, The density functional formalism, its applications and prospects, *Rev. Mod. Phys.*, 1989, **61**, 689–746.